Effective time-reversal symmetry breaking in the spin relaxation in a graphene quantum dot

P. R. Struck and Guido Burkard
Department of Physics, University of Konstanz, D-78457 Konstanz, Germany
(Received 6 August 2010; published 1 September 2010)

We study the relaxation of a single electron spin in a circular gate-tunable quantum dot in gapped graphene. Direct coupling of the electron spin to out-of-plane phonons via the intrinsic spin-orbit coupling leads to a relaxation time T_1 which is independent of the B field at low fields. We also find that Rashba spin-orbit induced admixture of opposite spin states in combination with the emission of in-plane phonons provides various further relaxation channels via deformation potential and bond-length change. In the absence of valley mixing, spin relaxation takes place within each valley separately and thus time-reversal symmetry is effectively broken, therefore inhibiting the Van Vleck cancellation at $B=0$ known from GaAs quantum dots. Both the absence of the Van Vleck cancellation as well as the out-of-plane phonons lead to a behavior of the spin-relaxation rate at low magnetic fields which is markedly different from the known results for GaAs. For low-B fields, we find that the rate is constant in B and then crosses over to $\propto B^2$ or $\propto B^4$ at higher fields.

DOI: 10.1103/PhysRevB.82.125401 PACS number(s): 73.63.Kv, 03.67.Lx, 72.25.Rb, 73.22.Pr

I. INTRODUCTION

The electronic spin degree of freedom is under intense investigation as a possible implementation of a qubit.[1] While the feasibility of all required operations has been experimentally demonstrated for GaAs quantum dots (QDs),[2] the decoherence caused by the surrounding nuclear spins in the host material remains challenging. Regarding the use of the electron spin as a qubit in quantum computation devices, spin decoherence and relaxation are limiting factors. In general, a necessary condition for a working qubit is that the time required to perform an operation is significantly shorter than the decoherence and relaxation times. Motivated by this, the implementation of qubits in QDs in graphene has been proposed.[3] Graphene consisting of natural carbon comprises 99% of the carbon isotope ^{12}C which has no nuclear spin, hence the hyperfine interaction is expected to play only a minor role. Furthermore, spin-orbit interaction (SOI) in graphene is expected to be relatively weak and therefore long decoherence times are expected. However, for spins localized in QDs in carbon nanotubes, SOI has turned out to be unexpectedly strong[4,5] due to curvature-induced effects. It has also been shown theoretically that Van Hove singularities in the phonon density of states in one dimension can lead to strong variations in the spin-relaxation rate.[6] It is therefore important to investigate the spin-relaxation time in graphene QDs. The form of the SOI in graphene, both intrinsic and Rashba type, has been derived from symmetry arguments[7] as well as tight-binding calculations.[8,9] It was predicted that the spin-relaxation rate of extended states depends on various parameters such as curvature or electric field.[8,10] Furthermore, there have also been experimental[11] and theoretical[12] studies on spin relaxation of extended states in graphene.

In this paper we determine theoretically the spin-relaxation time T_1 for an electron confined to a circular QD in gapped graphene as a function of the external magnetic field **B**. It has been predicted previously that such QDs can be formed with electrostatic confinement in either single-layer graphene with a substrate-induced band gap or bilayer graphene with an electrically controlled gap.[13] At $\mathbf{B}=0$, the states in these QDs have a twofold valley degeneracy which can be lifted in a perpendicular magnetic field. Being a centrosymmetric crystal, phonons in graphene do not couple piezoelectrically, thus leaving three possible electron-phonon coupling (EPC) mechanisms: deformation potential, bond-length change, and direct spin-phonon coupling. From these EPC mechanisms, we derive two spin-relaxation mechanisms. One such mechanism involves the admixture of states of opposite spin and excited orbitals into the dot eigenstates due to SOI, in combination with energy relaxation via phonon emission.[14,15] It turns out that to lowest order in the EPC, this only involves in-plane phonons coupled via the deformation potential and bond-length change. The second mechanism directly couples the spin to out-of-plane phonons via curvature-induced SOI. For comparison, in a parabolic GaAs QD, a strong dependence $\propto B^5$ has been predicted for both mechanisms.[14] Relaxation times in the millisecond range at a field $B=1$ T have been predicted and even longer T_1 exceeding one second have been experimentally verified.[16] The prediction for graphene QDs looks markedly different because of the absence of the Van Vleck cancellation for spin qubits

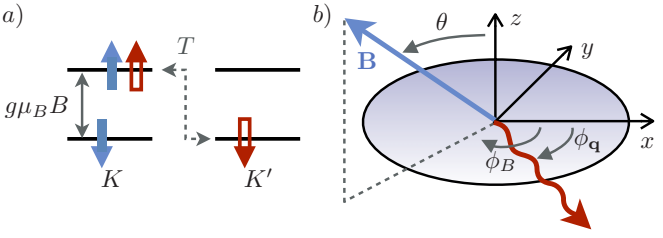

FIG. 1. (Color online) (a) The two states of a *spin qubit* (blue solid arrows) reside in the same valley, as opposed to a *Kramers qubit* (empty red arrows), formed by a Kramers pair related by time-reversal symmetry (T). While in single-valley semiconductors such as GaAs these two cases are identical, in graphene the Kramers qubit involves states in different valleys (K and K'). (b) The B-field orientation is given with spherical coordinates θ and ϕ_B relative to the normal to the graphene plane. The propagation direction of the emitted phonon (red wavy arrow) is described by the angle ϕ_q.

in a single valley as opposed to "Kramers qubits" [see Fig. 1(a)], as well as the absence of piezophonons and the two-dimensional (2D) nature of phonons.

II. MODEL

To study spin relaxation in a circular and gate-tunable QD in single-layer graphene, we assume the host graphene layer to be sufficiently large to ensure that the edges do not induce intervalley mixing. The QD can be described with the Hamiltonian,[13]

$$H_0 = v_F(\mathbf{p} + e\mathbf{A}_\perp)\cdot\boldsymbol{\sigma} + \frac{1}{2}g\mu_B\mathbf{B}\cdot\mathbf{s} + U(r) + \tau\Delta\sigma_z, \quad (1)$$

where the first term is the well-known Dirac Hamiltonian for graphene[17] in the presence of a vector potential $\mathbf{A}_\perp$ with $\mathbf{B}_\perp = \nabla\times\mathbf{A}_\perp = (0,0,B\cos\theta)$ being the perpendicular component of an arbitrarily oriented B field [Fig. 1(b)]. The second and third terms describe the Zeeman coupling of the electron spin to the total B field and the smooth and finite circularly symmetric confinement potential $U(r) = U_0\theta(r-R)$. Due to the two-dimensional electron gas (2DEG) living on the very surface and therefore very close to the top gates such a potential can be created much better in graphene than in GaAs.[18]

The last term opens a band gap 2Δ which can, e.g., arise due to the influence of a BN or SiC substrate, or a monolayer of intercalated Au on Ru(0001).[19–21] Here, $\tau = \pm 1$ denote the K and K' valleys. In the absence of valley scattering, we can restrict ourselves to a single valley, e.g., $\tau = +1$. Weak intervalley coupling can arise from atomic defects or boundaries,[17] or from the hyperfine interaction with the remaining ^{13}C atoms.[22]

The eigenstates $|n,s\rangle^{(0)}$ of H_0 in Eq. (1) with energy $E_n + sg\mu_B B/2$ are simultaneously eigenstates of the total angular momentum $j \in \mathbb{Z} + \frac{1}{2}$, i.e., orbital quantum number and pseudospin with spinor wave functions (in the K valley),

$$\langle r,\phi|n;s\rangle = \psi_n(r,\phi) = e^{i(j-1/2)\phi}\begin{pmatrix}\chi_A^{j,\nu}(r)\\ \chi_B^{j,\nu}(r)e^{-i\phi}\end{pmatrix}. \quad (2)$$

The spinor components $\chi_\sigma^{j,\nu}(r)$ can be given in closed form for a steplike potential $U(r)$ as introduces above,[13] however the eigenenergies E_n have to be evaluated numerically. Each eigenstate is characterized by a pair (n,s), where $s = \uparrow, \downarrow = \pm 1$ is the spin and where $n = (\nu, j)$ has a radial and angular momentum part.

III. IN-PLANE PHONONS

In order to study processes based on the admixture mechanism, we begin with the Hamiltonian $H = H_0 + H_{\mathrm{SO}} + H_{\mathrm{EPC}}$, where H_0 describes the graphene QD without SOI as explained above, H_{SO} describes the SOI, and H_{EPC} describes EPC. The effect of the SOI is to weakly mix the eigenstates Eq. (2). In this manner, e.g., the QD ground state, say, $|n = (0,1/2),\uparrow\rangle^{(0)}$ acquires components of the excited states $|n',\downarrow\rangle^{(0)}$ with $n' = (\nu', j') \neq n$ and opposite spin, to first order in H_{SO},

$$|n\uparrow\rangle = |n\uparrow\rangle^{(0)} + \sum_{n'\neq n}\frac{{}^{(0)}\langle n'\downarrow|H_{\mathrm{SO}}|n\uparrow\rangle^{(0)}}{E_n - E_{n'} - \frac{1}{2}g\mu_B B}|n'\downarrow\rangle^{(0)} \quad (3)$$

and similarly for $|n\downarrow\rangle$. With this admixed state the spin-conserving EPC can cause spin relaxation,

$$\begin{aligned}\langle n\uparrow|H_{\mathrm{EPC}}|n\downarrow\rangle &\equiv (H_{\mathrm{EPC}})_{nn}^{\uparrow\downarrow}\\ &= \sum_{n'\neq n}\left[\frac{(H_{\mathrm{SO}})_{nn'}^{\uparrow\downarrow}(H_{\mathrm{EPC}})_{n'n}}{E_n - E_{n'} - \frac{1}{2}g\mu_B B} + \frac{(H_{\mathrm{EPC}})_{nn'}(H_{\mathrm{SO}})_{n'n}^{\uparrow\downarrow}}{E_n - E_{n'} + \frac{1}{2}g\mu_B B}\right].\end{aligned} \quad (4)$$

For sufficiently small B fields this can be expanded around $B=0$. In the case of GaAs, the expression (4) vanishes for $B=0$ due to the symmetry $(H_{\mathrm{SO}})_{nm}^{\uparrow\downarrow} = -(H_{\mathrm{SO}})_{mn}^{\uparrow\downarrow}$ and $(H_{\mathrm{EPC}})_{nm} = (H_{\mathrm{EPC}})_{mn}$. This Van Vleck cancellation[14,15] is one of the reasons for the high power of B that appears in the spin-relaxation rate in GaAs QDs and can be traced back to the time-reversal invariance of H and its eigenstates, i.e., the fact that both SOI and EPC preserve time-reversal invariance. In particular, the spin relaxation takes place from one state, say, $|n\uparrow\rangle$, to its partner $|n\downarrow\rangle$ within a Kramers pair, which are linked by time reversal.

In our case, the states $|n\uparrow\rangle$ and $|n\downarrow\rangle$ lie in the same valley and therefore do not form a Kramers pair [see Fig. 1(a)]. The time-reversed partner of $|n\uparrow\rangle$ is $|n\downarrow\rangle'$, where the prime denotes the opposite valley. Since neither the EPC nor the SOI lead to intervalley mixing, spin relaxation is effectively constrained to a single valley. Therefore the selection of spin qubit states within the same valley breaks time-reversal symmetry and leads to the absence of the Van Vleck cancellation. We now proceed to the evaluation of the matrix elements of the SOI and the EPC in Eq. (4) in order to calculate the spin-relaxation rate.

We divide the SOI Hamiltonian into its intrinsic and Rahsba terms,[7]

$$H_{\mathrm{SO}} = H_i + H_R = \Delta_i\tau\sigma_z s_z + \Delta_R(\tau\sigma_x s_y - \sigma_y s_x), \quad (5)$$

where σ_i and s_i denote the Pauli matrices acting on the pseudospin and real spin. We use a spin quantization axis aligned with the external B field [see Fig. 1(b)] and corresponding spinors $|\uparrow_B\rangle$ and $|\downarrow_B\rangle$ and obtain

$$f_x \equiv \langle\uparrow_B|s_x|\downarrow_B\rangle = \cos^2\frac{\theta}{2} - e^{-2i\phi_B}\sin^2\frac{\theta}{2}, \quad (6)$$

$$f_y \equiv \langle\uparrow_B|s_y|\downarrow_B\rangle = -i\left(\cos^2\frac{\theta}{2} + e^{-2i\phi_B}\sin^2\frac{\theta}{2}\right). \quad (7)$$

First we consider H_R and calculate its matrix elements with states $|n\uparrow_B\rangle$ and $|n'\downarrow_B\rangle$. The two spin states we use are orthogonal, i.e., $\langle\uparrow_B|\downarrow_B\rangle = 0$ but they are not s_z eigenstates. In principle, this allows both the intrinsic and Rashba SOI to provide a relaxation channel in the admixture mechanism. However, due to the circular symmetry of the dot, selection rules for j apply. In the case of H_R only dipole transitions

($|j-j'|=1$) are allowed, whereas the matrix element of H_i gives rise to selection rules $j=j'$ which turns out to be incompatible with the selection rule $|j-j'|=1$ for the EPC.

The matrix element of H_R can be written as

$$(H_R)^{\uparrow\downarrow}_{nn'} = 2\pi\Delta_R[f^y(\delta_{jj'+1}N^{AB}_{nn'} + \delta_{jj'-1}N^{AB}_{n'n}) - if^x(\delta_{jj'+1}N^{AB}_{nn'} - \delta_{jj'-1}N^{AB}_{n'n})], \quad (8)$$

where $N^{AB}_{nn'}=\int dr r\chi^n_A\chi^{n'}_B$. The matrix element $(H_R)^{\uparrow\downarrow}_{nn'}$ is neither symmetric nor antisymmetric in contrast to the case of GaAs where an antisymmetry leads to Van Vleck cancellation.

We consider two different EPC mechanisms which correspond to different changes in the lattice induced by phonons. The deformation potential is caused by an area change in the unit cell, whereas the bond-length change mechanism corresponds to a modified hopping probability.[23,24] Because we work in the low-energy regime, we only consider acoustic phonons. In principle, there are six possible relaxation channels: (i) longitudinal-acoustic (LA), transversal-acoustic (TA), transversal out-of-plane (ZA) phonons, and (ii) deformation potential (g_1) and bond-length change (g_2) mechanisms. In lowest order in the atomic displacement, the EPC has the form[23,24]

$$H_{\rm EPC} = \frac{q}{\sqrt{A\rho\omega_{\mathbf{q},\mu}}}\begin{pmatrix} g_1a_1 & g_2a_2^* \\ g_2a_2 & g_1a_1 \end{pmatrix}(e^{i\mathbf{qr}}b^\dagger - e^{-i\mathbf{qr}}b) \quad (9)$$

with $a_1=i$ and $a_2=ie^{2i\phi_\mathbf{q}}$ for LA phonons, and $a_2=e^{2i\phi_\mathbf{q}}$ and $a_1=0$ for TA phonons, and A the area of the graphene sheet. The vanishing of a_1 is due to the fact that in the regime of linear atomic displacements the coupling of the TA mode is a two-phonon process. Here, we restrict our considerations to one-phonon processes. For a B field of $B=1$ T and a sound velocity of $s=2\times10^4$ m/s,[25] we obtain from $g\mu_BB=\hbar sq$ a phonon wavelength of $\lambda\approx300$ nm which is an order of magnitude larger than a typical QD size of 25 nm,[3] thus justifying the use of the dipole approximation for typical laboratory fields.

For the matrix element for LA phonon coupling via the deformation potential we find

$$(H^{\rm LA}_{\rm EPC})_{nn'} = -\frac{g_1\pi q^{3/2}M_{nn'}}{\sqrt{A\rho s_{\rm LA}}}(\delta_{jj'+1}e^{-i\phi_q} + \delta_{jj'-1}e^{i\phi_q}) \quad (10)$$

with $M_{nn'}=\int dr r^2(\chi^{n*}_A\chi^{n'}_A+\chi^{n*}_B\chi^{n'}_B)$. The dependence on the phonon-emission angle ϕ_q disappears upon summation over final states. For the TA phonons we find that the coupling via the deformation potential is a two-phonon process which will not be discussed here.

The bond-length change mechanism leads to similar results for both LA and TA phonons,

$$(H_{\rm EPC})_{nn'} = D_iq^{1/2}(\delta_{jj'+1}e^{-2i\phi_q}N^{AB}_{nn'} \pm \delta_{jj'-1}e^{i2\phi_q}N^{AB}_{n'n}) \quad (11)$$

with $D_{\rm LA}=-i2\pi g_2/\sqrt{A\rho s_{\rm LA}}$ and $D_{\rm TA}=2\pi g_2/\sqrt{A\rho s_{\rm TA}}$, and where the plus (minus) sign corresponds to LA (TA). In linear order in the atomic displacement the ZA mode is decoupled from the other modes. The Hamiltonian (9) cannot account for a coupling to the out-of-plane mode.

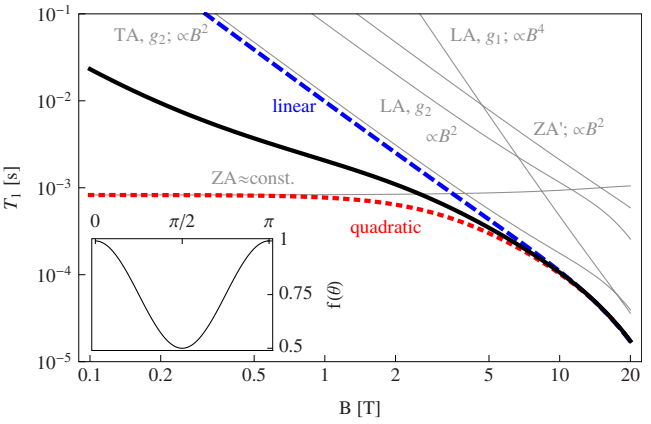

FIG. 2. (Color online) Log-log plot of the spin-relaxation time T_1 as a function of an external B field perpendicular to the plane ($\theta=0$) defined by the graphene sheet. The radius of the dot is $R=25$ nm and $\Delta=U_0=260$ meV. The individual relaxation channels are the coupling to LA in-plane phonons via deformation potential (g_1) and the coupling to LA and TA phonons via bond-length change (g_2). Also shown are the direct coupling to the out-of-plane phonons with quadratic (ZA) and linear (ZA′) dispersion. The red dotted, blue dashed, and solid black lines represent the sum of all four processes. For the red (blue) curve, a quadratic (linear) dispersion relation is assumed, while for the black curve a crossover from linear to quadratic is assumed (see text). Inset: dependence of the relaxation rate on the inclination angle θ of the B field.

With the matrix elements derived above, we can write the transition rates using Fermi's golden rule as

$$\frac{1}{T_1} \equiv \Gamma = 2\pi A\int\frac{d^2q}{(2\pi)^2}|(H_{\rm EPC})^{\uparrow\downarrow}_{nn}|^2\delta(sq-g\mu_BB). \quad (12)$$

For all mechanisms we find the same dependence on the orientation of the B field,

$$f(\theta) = \cos^4(\theta/2) + \sin^4(\theta/2) = [3+\cos(2\theta)]/4. \quad (13)$$

We find for the relaxation rate from the deformation potential,

$$\Gamma^{\rm LA}_{g_1} = \frac{16\pi^4g_1^2\Delta_R^2}{\rho}\frac{(g\mu_BB)^4}{s^6_{\rm LA}}f(\theta) \times\left|\sum_{n'\neq n}M_{nn'}R_{nn'}(\delta_{jj'+1}N^{AB}_{nn'}+\delta_{jj'-1}N^{AB}_{n'n})\right|^2 \quad (14)$$

while for the bond-length change mechanism, we have

$$\Gamma^{\rm LA,TA}_{g_2} = \frac{64\pi^4g_2^2\Delta_R^2}{\rho}\frac{(g\mu_BB)^2}{s^4_{\rm LA,TA}}f(\theta) \times\left|\sum_{n'\neq n}R_{nn'}[\delta_{jj'+1}(N^{AB}_{nn'})^2+\delta_{jj'-1}(N^{AB}_{n'n})^2]\right|^2 \quad (15)$$

with $R_{nn'}=(E_n-E_{n'})^{-1}$. For numerical evaluation, we assume a QD size of $R=25$ nm and $\Delta=10\delta$, where $\delta=v/R$ is the average level distance. The depth of the quantum well is also

TABLE I. Individual relaxation rates in units of per second for LA phonons via the deformation potential at $B=1$ T. For higher quantum numbers ν, the rate decreases quickly.

	$\nu=1$	$\nu=2$	$\nu=3$
$j=-0.5$	1.1×10^{4}	2.6×10^{-2}	1.3×10^{-3}
$j=1.5$	1.6×10^{4}	1.2×10^{1}	9.3×10^{-2}

set to $U_0=10\delta$. The Rashba SOI constant can be adjusted by an external electric field[8] or by using different types of substrates. We chose a value of $\Delta_R=48$ μeV to calculate the relaxation times displayed in Fig. 2. For the EPC constants we assume $g_1=30$ eV and $g_2=1.5$ eV.[23] We use as sound velocities $s_{\mathrm{LA}}=1.95\times10^{4}$ m/s and $s_{\mathrm{TA}}=1.22\times10^{4}$ m/s.[25] The overlap integrals $N_{nn'}^{AB}$ and $M_{nn'}$ are calculated numerically. The sum over n' runs over all states, including the continuum. As shown in Table I, the contributions from higher levels vanish quickly so that we only take the first three levels into account. The relaxation rate $T_1=1/\Gamma$ is plotted in Fig. 2.

IV. DIRECT SPIN-PHONON COUPLING

In flat graphene the acoustic phonons with perpendicular (ZA) polarization are decoupled from the in-plane modes (LA, TA). We extend the SOI Hamiltonian (5) for the case of a graphene layer which is curved due to ZA phonons. For displacements much smaller than the wavelength the normal vector of the graphene plane can be written as $\hat{\mathbf{n}}(z)\approx\hat{\mathbf{z}}+\nabla u_z(x,y)$, where $u_z(x,y)$ is the displacement field representing the ZA phonons. Rotating the spin matrices into the local frame determined by the normal vector $\hat{\mathbf{n}}(z)$ we obtain in linear order in $u(z)$ a generalized SOI Hamiltonian $H_{\mathrm{SO}}=H_i+H_R$ with

$$H_i=H_i^{(0)}+\Delta_i(\partial_x u_z s_x+\partial_y u_z s_y)\sigma_z\tau, \tag{16}$$

$$H_R=H_R^{(0)}+\Delta_R(-\sigma_y\partial_x u_z+\tau\sigma_x\partial_y u_z)s_z, \tag{17}$$

where $H_i^{(0)}$ and $H_R^{(0)}$ are the SOI Hamiltonians for flat graphene given in Eq. (5). We evaluate these expressions for transverse out-of-plane (ZA) phonons, with a quadratic dispersion relation $\omega_{\mathbf{q}}=\mu q^2$, where $\mu=\sqrt{\kappa/\rho}$ with $\kappa=1.1$ eV the bending rigidity and $\rho=7.5\times10^{-7}$ kg/m^2 the mass area density.[25,26] The EPC Hamiltonian is then obtained by substituting the displacement operator for the ZA phonons $u_z=\sqrt{1/A\rho\omega_{\mathbf{q}}}(e^{i\mathbf{q}\cdot\mathbf{r}}b^{\dagger}+e^{-i\mathbf{q}\cdot\mathbf{r}}b)$ into Eqs. (16) and (17). For the intrinsic SOI we obtain the matrix element,

$$(H_i)_{nn}^{\uparrow\downarrow}=i\Delta_i\sqrt{1/A\rho\omega_{\mathbf{q}}}\langle n|\sigma_z e^{i\mathbf{q}\cdot\mathbf{r}}|n\rangle(q_x\langle\uparrow|s_x|\downarrow\rangle+q_y\langle\uparrow|s_y|\downarrow\rangle). \tag{18}$$

When evaluating the orbital matrix element only the lowest order in the dipole approximation contributes. All higher orders contain a factor $\propto e^{i\phi_{\mathbf{q}}}$ which averages to zero when the integration over $\phi_{\mathbf{q}}$ is carried out.

Finally, Fermi's golden rule is used to find the relaxation rate,

$$\Gamma^{\mathrm{ZA}}=\frac{2\pi^2\Delta_i^2}{\rho\mu^2}f(\theta)\left|\int drr(|\chi_A^n|^2-|\chi_B^n|^2)\right|^2, \tag{19}$$

which depends only on B via the matrix element. For the numerical evaluation we use $\Delta_i=12$ μeV (Ref. 9) and $s_{\mathrm{ZA}}=1.59\times10^{3}$ m/s.[25] The same calculation for the Rashba SOI yields vanishing matrix elements and therefore no additional contribution. In some cases, boundary conditions may lead to a linear dispersion relation for the out-of-plane (ZA′) phonons. This contribution is $\propto B^2$ but is negligible compared to the in-plane phonon contributions as seen in Fig. 2. We also calculate the case in which the dispersion relation is of the form $\hbar\omega=\hbar sq+\hbar\mu q^2$. In order to show the crossover behavior of T_1 in the regime where both quadratic and linear-dispersion relation play an equal role, we have assumed a sound velocity of $s_{\mathrm{ZA}}=0.25\times10^{3}$ m/s.

V. CONCLUSION

We have calculated the electron-spin-relaxation time T_1 in a gate-tunable graphene QD arising from the combination of SOI and EPC. We have restricted ourselves to the zero-temperature case, i.e., pure phonon emission which is realistic at 0.1 T and 100 mK and higher temperatures for larger fields. We have taken into account two mechanisms: admixture mechanism and direct spin-phonon coupling. Due to selection rules in a circular QD, the admixture mechanism only leads to spin relaxation in combination with the Rashba SOI. The deformation-potential EPC with LA phonons leads to a spin-relaxation rate scaling as B^4 (Fig. 2) while the bond-length change EPC with both LA and TA phonons results in B^2 dependencies. The relatively low powers compared to GaAs QDs can be traced back to the absence of the Van Vleck cancellation, in combination with the 2D phonon density of states. The direct coupling of electronic spins to ZA phonons only leads to spin relaxation in combination with the intrinsic SOI whose rate does not depend on the applied B field (in lowest order) and thus leads to a B-field dependence at low fields which is markedly different from that in GaAs QD.

ACKNOWLEDGMENTS

We thank András Pályi for useful discussions and we acknowledge funding from the DFG within FOR 912 "Coherence and Relaxation Properties of Electron Spins."

[1] D. Loss and D. P. DiVincenzo, Phys. Rev. A **57**, 120 (1998).
[2] R. Hanson, L. P. Kouwenhoven, J. R. Petta, S. Tarucha, and L. M. K. Vandersypen, Rev. Mod. Phys. **79**, 1217 (2007).
[3] B. Trauzettel, D. V. Bulaev, D. Loss, and G. Burkard, Nat. Phys. **3**, 192 (2007).
[4] F. Kuemmeth, S. Ilani, D. C. Ralph, and P. L. McEuen, Nature (London) **452**, 448 (2008).
[5] H. O. H. Churchill, F. Kuemmeth, J. W. Harlow, A. J. Bestwick, E. I. Rashba, K. Flensberg, C. H. Stwertka, T. Taychatanapat, S. K. Watson, and C. M. Marcus, Phys. Rev. Lett. **102**, 166802 (2009).
[6] D. V. Bulaev, B. Trauzettel, and D. Loss, Phys. Rev. B **77**, 235301 (2008).
[7] C. L. Kane and E. J. Mele, Phys. Rev. Lett. **95**, 226801 (2005).
[8] H. Min, J. E. Hill, N. A. Sinitsyn, B. R. Sahu, L. Kleinman, and A. H. MacDonald, Phys. Rev. B **74**, 165310 (2006).
[9] M. Gmitra, S. Konschuh, C. Ertler, C. Ambrosch-Draxl, and J. Fabian, Phys. Rev. B **80**, 235431 (2009).
[10] D. Huertas-Hernando, F. Guinea, and A. Brataas, Phys. Rev. B **74**, 155426 (2006).
[11] N. Tombros, C. Jozsa, M. Popinciuc, H. T. Jonkman, and B. J. van Wees, Nature (London) **448**, 571 (2007).
[12] D. Huertas-Hernando, F. Guinea, and A. Brataas, Phys. Rev. Lett. **103**, 146801 (2009).
[13] P. Recher, J. Nilsson, G. Burkard, and B. Trauzettel, Phys. Rev. B **79**, 085407 (2009).
[14] A. V. Khaetskii and Y. V. Nazarov, Phys. Rev. B **64**, 125316 (2001).
[15] J. H. Van Vleck, Phys. Rev. **57**, 426 (1940).
[16] S. Amasha, K. MacLean, I. P. Radu, D. M. Zumbühl, M. A. Kastner, M. P. Hanson, and A. C. Gossard, Phys. Rev. Lett. **100**, 046803 (2008).
[17] A. H. Castro Neto, F. Guinea, N. M. R. Peres, K. S. Novoselov, and A. K. Geim, Rev. Mod. Phys. **81**, 109 (2009).
[18] N. Gu, M. Rudner, A. Young, P. Kim, and L. Levitov, arXiv:1003.2399 (unpublished).
[19] G. Giovannetti, P. A. Khomyakov, G. Brocks, P. J. Kelly, and J. van den Brink, Phys. Rev. B **76**, 073103 (2007).
[20] S. Y. Zhou, G.-H. Gweon, A. V. Fedorov, P. N. First, W. A. de Heer, D.-H. Lee, F. Guinea, A. H. Castro Neto, and A. Lanzara, Nature Mater. **6**, 770 (2007).
[21] C. Enderlein, Y. S. Kim, A. Bostwick, E. Rotenberg, and K. Horn, New J. Phys. **12**, 033014 (2010).
[22] A. Pályi and G. Burkard, Phys. Rev. B **80**, 201404 (2009).
[23] T. Ando, J. Phys. Soc. Jpn. **74**, 777 (2005).
[24] E. Mariani and F. von Oppen, Phys. Rev. Lett. **100**, 076801 (2008).
[25] L. A. Falkovsky, Phys. Lett. A **372**, 5189 (2008); see also arXiv:cond-mat/0702409; JETP **105**, 397 (2010).
[26] D. Gazit, Phys. Rev. B **79**, 113411 (2009).